

Very High Energy Flat Spectral Radio Quasar Candidates

Malik Zahoor^{1*}, Sunder Sahayanathan^{2,3†}, Shah Zahir^{4‡}, Naseer Iqbal¹, Aaqib Manzoor¹

¹Department of Physics, University of Kashmir, Srinagar 190006, India.

²Astrophysical Sciences Division, Bhabha Atomic Research Center, Mumbai 400085, India.

³Homi Bhabha National Institute, Mumbai 400094, India.

⁴Department of Physics, Central University of Kashmir, Ganderbal 191201, India.

Accepted XXX. Received YYY; in original form ZZZ

ABSTRACT

The attenuation of very high energy (VHE) photons by the extragalactic background light (EBL) prevents the observation of high redshift flat spectrum radio quasars (FSRQs). However, the correlation of VHE spectral index with source redshift suggests that EBL intensity may be less than what is predicted. This deviation can draw new constraints on opacity of the universe to VHE gamma-rays. Therefore, more FSRQs may fall above the sensitivity of the forthcoming VHE telescopes than the ones predicted by the existing EBL models. In order to account for the lower EBL intensity predicted by the index-redshift correlation, we introduce a redshift dependent correction factor to the opacity estimated from commonly used cosmological EBL model. Considering this modified opacity, we identify the plausible VHE FSRQ candidates by linearly extrapolating the *Fermi* gamma-ray spectrum at 10 GeV to VHE regime. Our study suggests among 744 FSRQs reported in *Fermi* fourth catalog-Data release 2 (4FGL-DR2), 32 FSRQs will be detectable by Cherenkov Telescope Array Observatory (CTAO). Since the FSRQs are proven to be highly variable, we assume a scenario where the average *Fermi* gamma-ray flux increases by a factor of 10 and this predicts additional 90 FSRQs that can be detected by CTAO.

Key words: gamma rays: galaxies – galaxies: active – cosmic background radiation

1 INTRODUCTION

Very high-energy (VHE, $E > 100\text{GeV}$) gamma-ray astronomy have the potential to provide unique insights on open issues related to cosmology and particle physics. Additionally, it serves as an important probe for multi-wavelength and multi-messenger astronomy. VHE emission from the astrophysical sources can be observed from the ground by studying the shower of secondary charged particles initiated through the interaction of the primary gamma-rays with the atmosphere (de Naurois & Mazin 2015). Among various techniques employed, the Imaging Atmospheric Cherenkov Telescopes (IACTs) detect the primary gamma-rays through the image of the Cherenkov pool caused by the secondary shower. The current-generation IACTs, which include *HESS* (Aharonian et al. 2006), *MAGIC* (Aleksić et al. 2012), and *VERITAS* (Holder et al. 2006), have been contributing extensively to VHE astrophysics for nearly two decades. In tandem with the telescopes operating at other energies (e.g. *Fermi*-LAT (Atwood et al. 2009), *Swift* (Burrows et al. 2005), *NuSTAR* (Harrison et al. 2013) and *XMM-Newton* (Jansen et al. 2001)), IACTs have provided clues to understand the non-thermal emission processes in blazars (Knödlseder 2016).

The advent of new generation ground-based VHE telescopes, including the proposed Cherenkov Telescope Array Observatory (CTAO) (Cherenkov Telescope Array Consortium et al. 2019), the gamma-ray astronomy is entering into a new era. Operating from

a few tens of GeV to the multi-TeV energy band, the CTAO is designed to be the largest and the most sensitive gamma-ray observatory in this energy range (Gueta 2021). It will be configured as two sets of Cherenkov telescope arrays, one in each of the Earth’s hemispheres, and it is expected to start science operations at full capacity within few years. CTAO along with other upcoming VHE experiments, the Large High Altitude Air Shower Observatory (*LHAASO*) (Cao 2021), *ASTRI* Mini-Array (*ASTRI MA*) (Antonelli 2021), Southern Wide-field Gamma-ray Observatory (*SWG0*) (Barres de Almeida et al. 2021), Major Atmospheric Cherenkov Experiments (*MACE*) (HiGRO Collaboration et al. 2021) etc, will be able to explore the gamma-ray sky with unprecedented performance, notably in the multi-TeV energy range.

Blazars dominate the extragalactic sky at VHE energies. These objects are the subclass of Radio loud active galactic nuclei (AGNs) having a relativistic jet pointing close to the line of sight of the observer on earth (Urry & Padovani 1995). The spectral energy distribution (SED) of blazars is dominated by the non thermal emission from the jet and consists of two broad peaks. The low energy component extends from radio-to-X-rays and is attributed to the synchrotron emission, while the high energy component is commonly interpreted as the inverse Compton (IC) scattering of low energy photons by the relativistic electron distribution in the jet (Urry & Padovani 1995). Blazars are further classified into BL Lac objects and Flat spectrum radio Quasars (FSRQs) based on the presence/absence of broad emission/absorption line features in their optical spectra. The synchrotron SED of BL Lacs generally peaks at optical-to-X-ray energies; whereas, for FSRQs this spectral peak fall in infrared-optical

* E-mail: malikzahoor313@gmail.com

† E-mail: sunder@barc.gov.in

‡ E-mail: shahzahir4@gmail.com

energy range. Besides the variation in peak location, the IC component of blazars is significantly different for BL Lacs and FSRQs. Particularly, the IC luminosity for FSRQs is larger than the synchrotron luminosity, commonly referred as *Compton dominance*, while it is of similar order in case of BL Lacs (Sikora et al. 1994). The target photon field for the IC process is also different for these two class of blazars. The IC scattering of synchrotron photons (synchrotron self Compton mechanism: SSC) is quite successful in explaining the Compton spectral component of BL Lacs. However, modelling the high energy SED of FSRQs through IC mechanism demands additional photon field other than synchrotron emission. This photon field can be external to the jet and the plausible sources are the thermal photons from the accretion disc (Dermer & Schlickeiser 1993), broad emission line photons (Błażejowski et al. 2000) and/or the IR photons from the dusty torus (Sikora et al. 1994).

The interaction of VHE gamma-rays with the extragalactic background light (EBL) results in the formation of electron/positron pairs (Dwek & Krennrich 2013). The amount of attenuation depends on the redshift of the source and the energy of the VHE photons. For distant blazars, this causes the observed VHE spectra to steepen, causing the flux to fall below the telescope sensitivity. Consequently this makes the Universe opaque above few tens of GeV for objects having larger redshifts (gamma-ray horizon) which was initially predicted at $z > 0.1$ (Gould & Schröder 1967). Improved sensitivity of the current generation Cherenkov telescopes and better estimation of EBL intensity have significantly modified the gamma-ray horizon; nevertheless, detection of the FSRQs 4FGL J0221.1+3556 and 4FGL J1443.9+2501 located at redshifts 0.954 (Ahnen et al. 2016) and 0.939 (Abeysekara et al. 2015; Ahnen et al. 2015) suggest the EBL intensity may still be less than the prediction.

Knowledge of EBL intensity and the intrinsic source VHE spectrum is crucial in identifying the VHE blazar candidates. The latter is often estimated by extrapolating the *Fermi* high energy gamma-ray spectrum to VHE energies (Paiano et al. 2021; Zhu et al. 2021). The VHE blazar candidates are then obtained by convolving the extrapolated spectrum with EBL induced opacity predicted through cosmological models. However, such candidates are put forth only for BL Lacs (Massaro et al. 2013; Foffano et al. 2019; Balmaverde et al. 2019; Costamante 2019; Paiano et al. 2021; Zhu et al. 2021) and no such study have been performed for FSRQs. The primary reason being, the *Fermi* spectrum of FSRQs generally deviate from a power-law and is often represented by a log-parabolic function, and extending this function to VHE energies roll off the spectrum significantly. Additionally, the FSRQs are populated at higher redshifts and the current EBL models disfavour them as probable candidates. Besides this, most VHE detections of FSRQs have been during enhanced flux states and hence the flux variability plays a crucial role in VHE studies of these sources.

In our earlier study (Malik et al. 2022) (hereafter Paper I), using the correlation between observed VHE spectral index with the redshift, we have highlighted the deviation of different cosmological EBL models from the observations. The important assumptions in the earlier study are: a) The average intrinsic VHE spectral index is consistent with the regression line extrapolated to redshift, $z=0$, b) The spectral index variation of the individual source is much smaller than the steepening introduced by EBL at large redshifts, and c) The cosmological evolution of the source do not modify the intrinsic VHE spectral indices. This study suggests the EBL intensity may be much less intense than the ones predicted by the cosmological models. Consistently, this also suggests the gamma-ray horizon may fall at much larger redshifts than the one presumed. Moreover, from the X-ray spectral studies of blazars it is known that the log-parabolic

function is successful in reproducing only a narrow energy band (Massaro et al. 2004). Hence, it may not be judicious to expect the *Fermi* log-parabolic spectral shape to extend up to VHE. In this work, we predict the plausible VHE FSRQ candidates considering these discrepancies. We perform a linear extrapolation of the high energy spectrum of FSRQs listed in 4FGL-DR2 catalog (Ballet et al. 2020) to VHE as a prediction for the intrinsic VHE spectra. To account for the reduction in EBL intensity, suggested by VHE observations of FSRQs (Paper I), we add a redshift dependent correction factor to the EBL opacity provided by Franceschini & Rodighiero (2017) (hereafter FM). These modifications are then used to predict the list of VHE FSRQs that can be studied by CTAO and other operational Cherenkov telescopes. In the next section §2 we first introduce a correction factor to the existing EBL estimates (using Paper I) followed by intrinsic VHE flux estimations using *Fermi* spectral information. The section concludes by over-plotting the sensitivity curves of present and upcoming VHE telescopes to look for the possible VHE FSRQ candidates. Finally the Results are summarised and discussed in section §3. In this work we adopt a cosmology with $\Omega_M = 0.3$, $\Omega_\Lambda = 0.7$, and $H_0 = 71 \text{ km s}^{-1} \text{ Mpc}^{-1}$.

2 VHE FSRQ CANDIDATES

2.1 Modified EBL Photon Density

The VHE detection of large redshift FSRQs indicate the Universe may be more transparent to VHE gamma-rays than anticipated. A similar conclusion is also drawn from the correlation study between the observed VHE spectral index and the redshift (Paper I). These results suggest, the predicted EBL intensity at large redshifts may be considerably larger than the actual value. To account for this excess, we introduce a redshift dependent correction factor $a(z)$ to the commonly used EBL opacity $\tau(E, z)$ by FM,

$$\tau_c(E, z) = a(z)\tau(E, z) \quad (1)$$

where, τ_c is the corrected opacity (hereafter modified FM; MFM) and E is the VHE photon energy. This correction factor will result in a harder observed VHE spectral index Γ_{obs} for a putative intrinsic spectrum (Figure 1) given by Paper I,

$$\Gamma_{\text{obs}} = \Gamma_{\text{int}} + a(z) \frac{d\tau}{d \ln(E)} \quad (2)$$

where, Γ_{int} is the intrinsic VHE spectral index and $a(z) < 1$. Estimation of $a(z)$ demands the knowledge of Γ_{int} which is obtained from the y-intercept of the best fit straight line to Γ_{obs} and z distribution (Paper I).

2.2 Intrinsic VHE Source Flux

The opacity of VHE photons, along with the correction factor, equation (1), let us to derive the observed flux of FSRQs provided the intrinsic flux is known. To estimate the latter we perform a linear extrapolation of the high energy spectrum of FSRQs to VHE. The information regarding the high energy spectrum is obtained from the fourth *Fermi* catalog, 4FGL-DR2 (Ballet et al. 2020). The data used in this catalog was collected over the period of ten years, starting from August 4 (15:43 UTC) in 2008 to August 2 in 2018 (19:13 UTC). It employs the same analysis methods as of 4FGL catalog (Abdollahi et al. 2020) in the energy range of 50 MeV to 1 TeV. Among 5788 sources listed in the catalog, 744 fall into the list of FSRQs. The attenuation due to EBL depends upon the source redshift

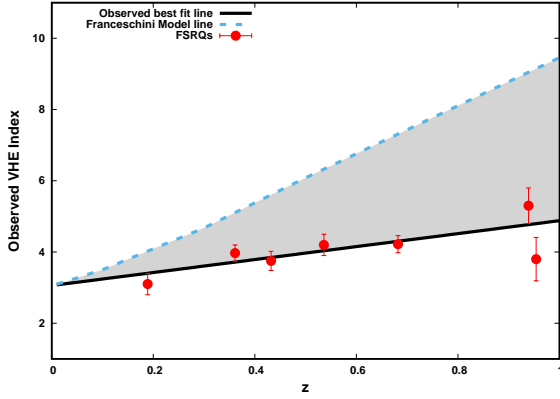


Figure 1. Comparison of observed VHE spectral indices with those estimated using EBL model by Franceschini & Rodighiero (2017) (FM) for FSRQs. The black solid line represents the best fit straight line to 7 FSRQs detected in VHE (Paper I), dashed line represents the index values estimated using FM. Grey region shows the deviation of EBL model from the observational best fit line to VHE indices.

and this is obtained from the online databases NED¹ and SIMBAD². These databases provide the redshifts of 586 FSRQs listed in 4FGL-DR2 and hence only these sources are considered for the present study. The information regarding the high energy spectrum of these FSRQs is extracted from the xml file available online³ and the same is plotted as a black dotted line in Figure 2.

The *Fermi* spectral behaviour for the selected sample of FSRQs is restricted to three distinct shapes. Among the 586 individual spectra of the sources, 263 are logparabola, 321 power-law and 2 sources exhibit a power-law with exponential cutoff. For the extrapolation to VHE band, we assume a power-law extension with index consistent with the spectral slope at 10 GeV (See Table 1 & 2). This energy is chosen since attenuation due to EBL is minimal below this energy for the range of redshifts considered (Ackermann et al. 2012), and the *Fermi* spectrum can be treated as true intrinsic spectrum. For 8 sources, we find the terminal *Fermi* power-law index is harder (≤ 2). Such hard indices suggest the Compton peak of these sources lie beyond the *Fermi* energy range and the VHE spectra can be much steeper than the one predicted by the power-law extrapolation. Hence we exclude these sources from this study. The extrapolated power law from the *Fermi* fit to the VHE band for the rest of sources is shown in Figure 2 as a red dotted line and this serves as the intrinsic VHE spectra F_{int} for the present study. The observed VHE spectrum F_{obs} is then obtained using τ_c from equation (1) (MFM)

$$F_{\text{obs}}(E, z) = F_{\text{int}}(E) e^{-\tau_c(E, z)} \quad (3)$$

The EBL attenuated VHE spectrum for the selected FSRQs using MFM is shown as solid black line in Figure 2. The attenuated spectrum considering FM is shown as green dotted line.

2.3 Comparison with IACT sensitivity

To identify the FSRQ candidates detectable by the operational and upcoming IACTs, we compare the predicted EBL attenuated VHE spectrum with the available sensitivity curves. The sensitivity curves of *CTAO*-South and North (Zenith Angle, $ZA < 20$ deg) are obtained

from the *CTAO* webpage⁴ while the sensitivity curve for *VERITAS* ($ZA < 40$ deg) is obtained from *VERITAS* webpage⁵. For other instruments such as *MAGIC* ($ZA < 35$ deg) and *H.E.S.S.* ($ZA < 18$ deg), the sensitivity curves are obtained from Aleksić et al. (2016) and Holler et al. (2016) respectively. These sensitivities are calculated at 5σ significance for 50 hours exposure time and are shown in Figure 2 with legends.

Comparing sensitivity of the IACTs and the predicted VHE spectrum of *Fermi* detected FSRQs, we identify the plausible VHE FSRQ candidates and list them in Table 1. Our study suggest, 32 FSRQs would fall within the detection threshold of *CTAO*'s Omega configuration (full-scope configuration), while the detection status with *CTAO*'s first construction phase (Alpha configuration) will be 29 using opacity estimates from MFM. Considering FM, the number of sources falling under the detection status of *CTAO* reduce to 23 and 20 for Omega and Alpha configurations of *CTAO* respectively. With the operational IACTs, the number of FSRQs falling within the detection threshold are 5 for *VERITAS* and 2 sources each for *MAGIC* and *HESS* using opacity estimates from MFM, while using FM the number of sources reduce to 2, 1 and 1 for *VERITAS*, *MAGIC* and *HESS* respectively (Table 1).

Blazars being extremely variable (Abdo et al. 2010; Meyer et al. 2019; Rajput et al. 2020), the intrinsic VHE flux derived from cumulative *Fermi* observations may portray only the average spectrum. To account for this variability, we assume a scenario where the VHE flux enhances by a factor of 10 above the prediction. Further, to be consistent with the rapid variability we use the *CTAO* sensitivity corresponding to 5 hour exposure time only. We refer the FSRQs which fall within the detection threshold of *CTAO* under this assumption as marginally detectable. In Table 2, we list the FSRQs which are marginally detectable and find additional 82 sources can be detected under Alpha configuration of *CTAO* for the opacity estimated by MFM. This number increases to 90 under Omega configuration of *CTAO*. For the opacity estimated from FM, the number of sources falling under the marginal detection list are 43 and 40 with Omega and Alpha configurations of *CTAO* respectively.

3 SUMMARY & DISCUSSION

The IACTs are narrow angle telescopes and require long duration observation of distant faint sources for significant detection. Hence, identification of plausible candidate FSRQs can provide a guideline for the upcoming VHE telescopes. Our earlier study, based on correlation between observed VHE spectral index with redshift (Paper I) suggests the universe may be more transparent to VHE photons than those predicted by cosmological EBL models. Taking cue from this, we predict the observed VHE fluxes of *Fermi* detected FSRQs and compare the same with the sensitivity of operational/upcoming telescopes. We find a significant number of FSRQs, listed in Table 1 and Table 2, can be studied by *CTAO* while few of them even with the operational IACTs. The sources which fall within the sensitivity limits of operational IACTs and are not reported in VHE yet are 4FGL J0043.8+3425 (*VERITAS*) and 4FGL J0957.6+5523 (*VERITAS*, *MAGIC*) (see Table 1). Among them 4FGL J0043.8+3425, is located at $z = 0.966$ which will be the second distant FSRQ if detected and only next to the newly announced 4FGL J0348.5-2749 at $z = 0.991$ (Wagner et al. 2021). However, the 10 GeV spectral index for

¹ <https://ned.ipac.caltech.edu/>

² <http://simbad.cfa.harvard.edu/simbad/>

³ https://fermi.gsfc.nasa.gov/ssc/data/access/lat/10yr_catalog/

⁴ <https://www.cta-observatory.org/science/cta-performance/>

⁵ <https://veritas.sao.arizona.edu/about-veritas/veritas-specification/>

this source is ~ 2.08 . Though this satisfies our selection criteria, the hard index suggests the Compton spectral peak may fall close to 10 GeV and hence the extrapolation can be questionable. Interestingly, the VHE emission from the FSRQ 4FGL J1159.5+2914, newly announced by *VERITAS* (Mukherjee & VERITAS Collaboration 2017) and *MAGIC* (Mirzoyan 2017) is also predicted to be a candidate source in this work (see Table 1). We also examined the detection status for *SWG0*, *LHAASO* and *MACE*, however we did not find any source falling within the detection threshold of these instruments.

Among the FSRQs predicted for CTAO, we find 11 sources at $z > 1$ fall under the detectable list and 33 under marginally detectable list (see Table 1,2). If detected, these high redshift sources may pose challenges to the existing cosmological EBL models. Alternatively, it can also play an important role in understanding the cosmology. Limits on EBL is mainly obtained through numerical models of the galaxy formation and/or their evolution with appropriate cosmological initial conditions (Domínguez et al. 2011). The model parameters are fine tuned to reproduce the observed universe. VHE identification of the sources at large redshifts can therefore be an important element to constrain the EBL which in turn can provide a better understanding about the galaxy formation and evolution. These identifications can also be used to test the alternate theories involving oscillation of photons and axion like particles proposed by the standard model (Irastorza & Redondo 2018; Galanti & Roncadelli 2018).

Considering the fact that the blazars are extremely variable (Abdo et al. 2010; Meyer et al. 2019; Rajput et al. 2020), certain FSRQs may still be detectable by operational/upcoming telescopes even though our study suggests otherwise. For instance, the FSRQ 4FGL J1422.3+3223 falls below our criteria for detection though it is detected at VHE (MAGIC Collaboration et al. 2021). This probably indicates that during the flaring epoch, the flux of this source can enhance more than 10 of its average flux. Consistently, we find the *Fermi* flux of 4FGL J1422.3+3223 during the VHE detection is typically more than 100 times larger than the average flux quoted in 4FGL catalog (Ciprini & Cheung 2020). Considering a similar factor of flux enhancement in the present work would make this source also as detectable by the operational IACTs *MAGIC* and *VERITAS*. Similar conclusion can be arrived for the newly announced FSRQ 4FGL J0348.5-2749 where the increase in *Fermi* flux, contemporaneous to the VHE detection, was ~ 200 times compared to average flux reported in *Fermi* 4FGL catalog (Wagner et al. 2021).

The VHE FSRQ candidates predicted in this work depend on the choice of $a(z)$ and the robustness of the regression line. However, the regression line is obtained by fitting merely 7 data points and this may deviate with future detections. Since the estimation of $a(z)$ assumes the intrinsic VHE index to be the y-intercept of the regression line, any deviation in the fit parameters can modify these predictions considerably. Conversely, a better regression analysis needs more FSRQs to be detected in VHE and the prediction based on the available information can facilitate this requirement. Detection of more VHE FSRQs with precise index measurements will also let us fit the redshift-index dependence with non-linear functions. Such a study will also have a major role in constraining the cosmological models.

VHE spectrum of FSRQs is better explained by a power-law function and hence we have assumed the intrinsic source spectrum also to be a power-law. If we consider the EC interpretation for the VHE emission, the Klein-Nishina effects will be substantial and the spectrum will deviate from a simple power-law (Dermer & Schlickeiser 1993). In addition, emission at VHE may involve high energy electrons that may fall close to the cut-off energy of the underlying electron distribution (Kirk et al. 1998). Under these conditions, the intrinsic VHE spectrum may deviate significantly from a power-

law and hence the powerlaw extrapolation to VHE energies can be an overestimate. Therefore these predictions on stringent conditions should be treated as an upper limit. The Klein-Nishina effect will depend upon the energy of the target photons and under extreme limits the VHE spectrum will be very steep with the photon spectrum nearly following the electron distribution (Blumenthal & Gould 1970). Hence, VHE study of FSRQs can also have the potential to understand the photon field environment of FSRQs.

4 ACKNOWLEDGEMENT

The authors thank the anonymous referee for valuable comments and suggestions. M.Z, S.S, N.I & A.M acknowledge the financial support provided by Department of Atomic energy (DAE), Board of Research in Nuclear Sciences (BRNS), Govt of India via Sanction Ref No.: 58/14/21/2019-BRNS. SZ is supported by the Department of Science and Technology, Govt. of India, under the INSPIRE Faculty grant (DST/INSPIRE/04/2020/002319). This research has made use of the CTA instrument response functions provided by the CTA Consortium and Observatory, see <https://www.cta-observatory.org/science/cta-performance/> (version prod3b-v2; <https://doi.org/10.5281/zenodo.5163273> and version prod5 v0.1; <https://doi.org/10.5281/zenodo.5499840>) for more details.

5 DATA AVAILABILITY

The codes and model used in this work will be shared on a reasonable request to the corresponding author Malik Zahoor (email: malikzahoor313@gmail.com).

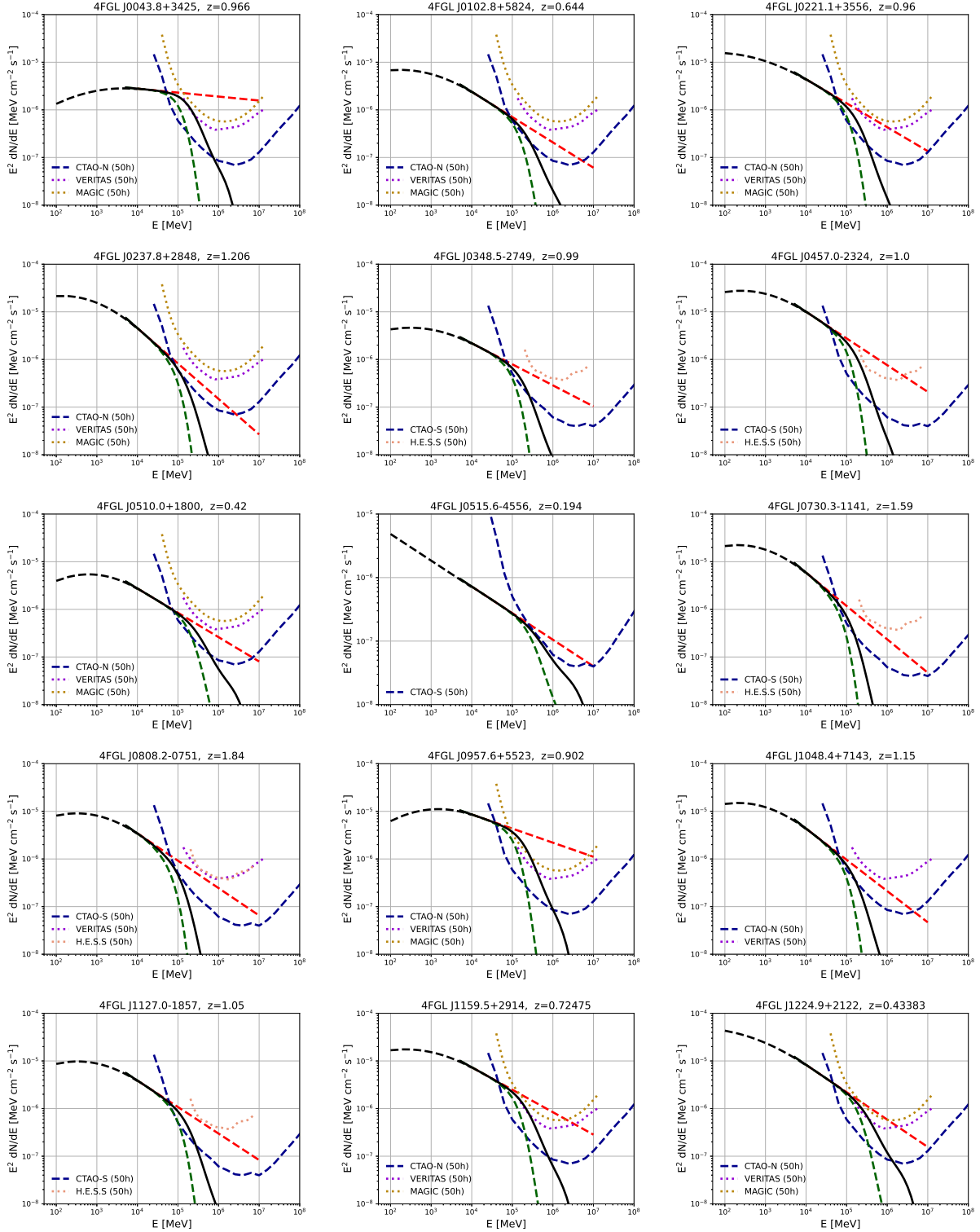


Figure 2. 32 VHE FSRQ candidates falling within the detection threshold of CTAO and other instruments. The black dashed line represents the *Fermi* 4FGL-DR2 spectral fit. Red dashed line shows the linear extrapolation of *Fermi* spectrum to VHE. The dashed green and solid black lines represent the EBL attenuated spectrum using [Franceschini & Rodighiero \(2017\)](#) (FM) and modified EBL model (MFM) respectively. The differential sensitivities of CTAO-North and South (Omega configuration, 50 hour), MAGIC (50 hour), VERITAS (50 hour) and H.E.S.S. (50 hour) are also plotted. Sensitivity curves are given in different colors as depicted in the Figure labels.

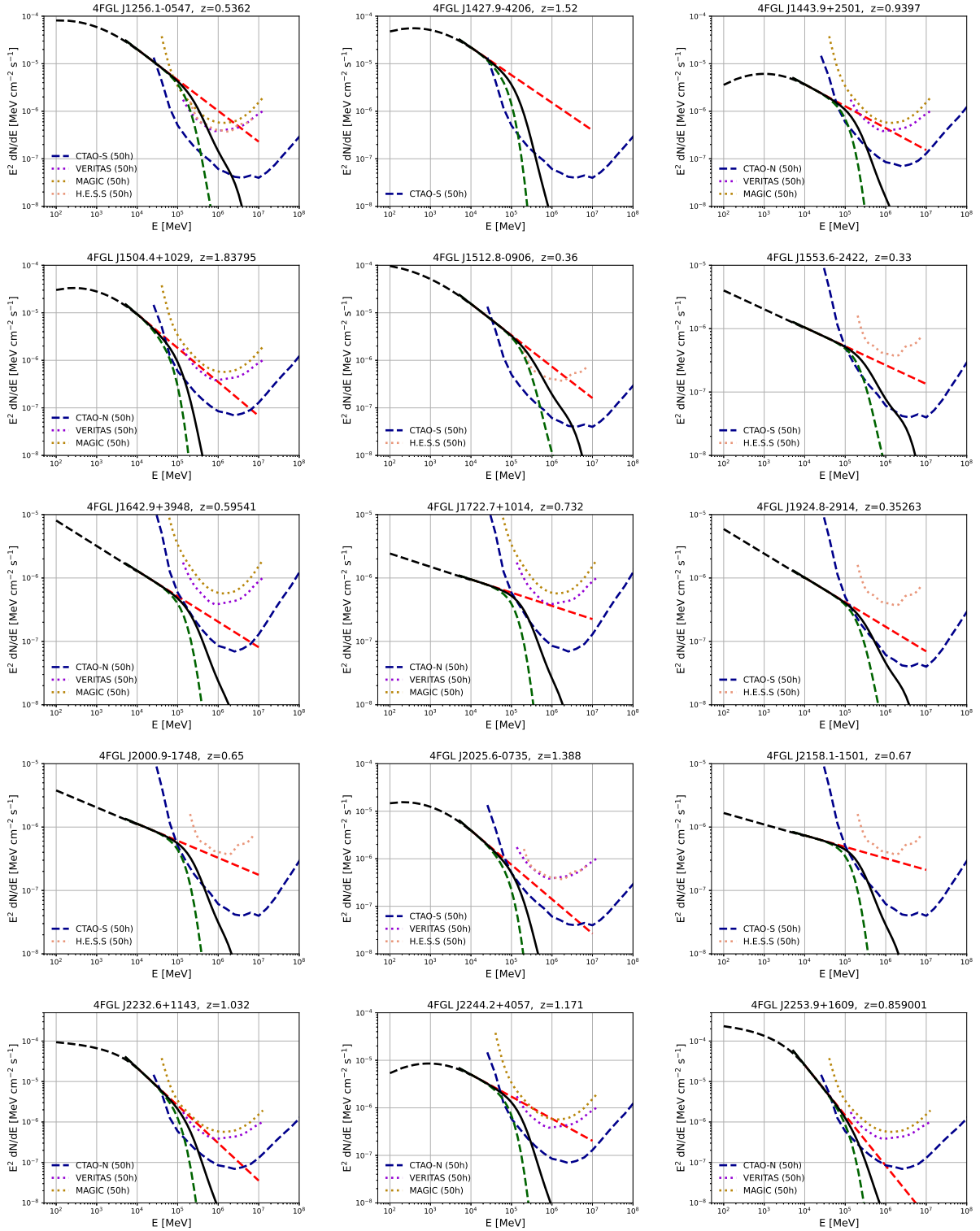


Figure 2 – continued

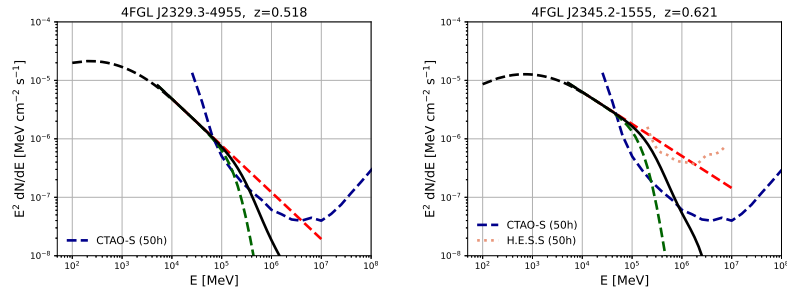


Figure 2 – continued

Table 1. List of VHE FSRQ candidates falling within the detection threshold of CTAO (Omega and Alpha configurations) and other IACTs. D and N depict "detected" and "non detected" sources corresponding to different instruments within 50 hours of exposure time. The FM and MFM corresponds to the detection status using opacity estimates from [Franceschini & Rodighiero \(2017\)](#) and modified EBL models respectively for each instrument.

Sourcename (4FGL-DR2)	R.A.	Decl.	Redshift	Spectral Slope (10 GeV)	CTAO (Omega)		CTA (Alpha)		VERITAS		MAGIC		HESS	
					MFM	FM	MFM	FM	MFM	FM	MFM	FM	MFM	FM
4FGL J0043.8+3425	00 43 53.2	+34 25 54	0.966	2.08	D	D	D	D	D	N	N	N	N	N
4FGL J0102.8+5824	01 02 48.2	+58 24 33	0.644	2.53	D	D	D	D	N	N	N	N	N	N
4FGL J0221.1+3556	02 21 07.4	+35 56 09	0.96	2.50	D	D	D	D	N	N	N	N	N	N
4FGL J0237.8+2848	02 37 53.7	+28 48 16	1.206	2.74	D	N	D	N	N	N	N	N	N	N
4FGL J0348.5-2749	03 48 34.0	-27 49 49	0.99	2.44	D	D	D	N	N	N	N	N	N	N
4FGL J0457.0-2324	04 57 02.6	-23 24 54	1.00	2.56	D	D	D	D	N	N	N	N	N	N
4FGL J0510.0+1800	05 10 04.3	+18 00 49	0.42	2.51	D	D	D	D	N	N	N	N	N	N
4FGL J0515.6-4556	05 15 37.4	-45 56 54	0.194	2.42	D	N	N	N	N	N	N	N	N	N
4FGL J0730.3-1141	07 30 18.6	-11 41 20	1.59	2.70	D	N	D	N	N	N	N	N	N	N
4FGL J0808.2-0751	08 08 15.6	-07 51 20	1.84	2.57	D	N	N	N	N	N	N	N	N	N
4FGL J0957.6+5523	09 57 39.9	+55 23 02	0.902000	2.30	D	D	D	D	D	D	D	N	N	N
4FGL J1048.4+7143	10 48 25.6	+71 43 47	1.1500	2.66	D	N	D	N	N	N	N	N	N	N
4FGL J1127.0-1857	11 27 03.2	-18 57 50	1.05	2.56	D	D	D	D	N	N	N	N	N	N
4FGL J1159.5+2914	11 59 32.2	+29 14 41	0.72475	2.47	D	D	D	D	D	N	N	N	N	N
4FGL J1224.9+2122	12 24 54.6	+21 22 53	0.43383	2.57	D	D	D	D	D	N	N	N	N	N
4FGL J1256.1-0547	12 56 10.0	-05 47 19	0.53620	2.65	D	D	D	D	D	D	D	D	D	N
4FGL J1427.9-4206	14 27 56.8	-42 06 22	1.52	2.58	D	D	D	D	N	N	N	N	N	N
4FGL J1443.9+2501	14 43 58.4	+25 01 45	0.9397	2.46	D	D	D	D	N	N	N	N	N	N
4FGL J1504.4+1029	15 04 24.8	+10 29 52	1.83795	2.71	D	D	D	D	N	N	N	N	N	N
4FGL J1512.8-0906	15 12 51.5	-09 06 23	0.36	2.66	D	D	D	D	N	N	N	N	D	D
4FGL J1553.6-2422	15 53 36.6	-24 22 07	0.33	2.30	D	D	D	D	N	N	N	N	N	N
4FGL J1642.9+3948	16 42 56.2	+39 48 59	0.59541	2.40	D	N	D	N	N	N	N	N	N	N
4FGL J1722.7+1014	17 22 44.6	+10 14 05	0.732	2.20	D	N	D	N	N	N	N	N	N	N
4FGL J1924.8-2914	19 24 51.3	-29 14 48	0.35263	2.38	D	D	D	N	N	N	N	N	N	N
4FGL J2000.9-1748	20 00 56.3	-17 48 59	0.65	2.27	D	D	D	N	N	N	N	N	N	N
4FGL J2025.6-0735	20 25 41.3	-07 35 40	1.388000	2.72	D	N	D	N	N	N	N	N	N	N
4FGL J2158.1-1501	21 58 06.6	-15 01 25	0.67	2.18	D	N	D	N	N	N	N	N	N	N
4FGL J2232.6+1143	22 32 36.6	+11 43 50	1.032	2.93	D	D	D	D	N	N	N	N	N	N
4FGL J2244.2+4057	22 44 14.7	+40 57 35	1.171	2.46	D	D	D	D	N	N	N	N	N	N
4FGL J2253.9+1609	22 53 59.1	+16 09 02	0.859001	3.24	D	D	D	D	N	N	N	N	N	N
4FGL J2329.3-4955	23 29 19.1	-49 55 57	0.518	2.80	D	D	D	D	N	N	N	N	N	N
4FGL J2345.2-1555	23 45 12.7	-15 55 06	0.621	2.55	D	D	D	D	N	N	N	N	N	N

Table 2. List of VHE FSRQ candidates falling within the marginal detection threshold of CTAO (Omega and Alpha configurations). M and N depict "marginally detected" and "non detected" sources corresponding to CTAO within 5 hours of exposure time. The FM and MFM corresponds to the detection status using opacity estimates from Franceschini & Rodighiero (2017) and modified EBL models respectively.

Sourcename (4FGL-DR2)	R.A.	Decl.	Redshift	Spectral Slope (10 GeV)	CTAO (Omega)		CTAO (Alpha)	
					MFM	FM	MFM	FM
4FGL J0038.2-2459	00 38 15.6	-24 59 24	0.49806	2.64	M	N	M	N
4FGL J0050.4-0452	00 50 26.9	-04 52 50	0.922	2.38	M	N	M	N
4FGL J0108.6+0134	01 08 40.7	+01 34 55	2.108898	2.89	M	M	M	M
4FGL J0112.8+3208	01 12 53.4	+32 08 24	0.6100	2.65	M	M	M	M
4FGL J0113.4+4948	01 13 28.4	+49 48 19	0.39	2.45	M	M	M	M
4FGL J0116.0-1136	01 16 00.1	-11 36 22	0.671	2.36	M	M	M	M
4FGL J0118.9-2141	01 18 54.1	-21 41 41	1.16	2.65	M	M	M	M
4FGL J0128.5+4440	01 28 34.5	+44 40 40	0.228	2.13	M	N	N	N
4FGL J0132.7-1654	01 32 42.2	-16 54 37	1.02	2.64	M	N	M	N
4FGL J0133.1-5201	01 33 10.5	-52 01 13	0.02	2.69	M	M	M	M
4FGL J0137.0+4751	01 37 02.5	+47 51 49	0.86	2.72	M	M	M	M
4FGL J0206.4-1151	02 06 24.4	-11 51 27	1.663	2.40	M	N	N	N
4FGL J0210.7-5101	02 10 46.7	-51 01 18	1.003	2.76	M	M	M	M
4FGL J0217.8+0144	02 17 50.9	+01 44 05	1.72	2.51	M	N	M	N
4FGL J0236.8-6136	02 36 48.5	-61 36 38	0.466569	2.35	M	M	M	M
4FGL J0252.8-2219	02 52 48.2	-22 19 13	1.419	2.80	M	N	M	N
4FGL J0253.5+3216	02 53 31.9	+32 16 57	0.859	2.17	M	N	M	N
4FGL J0259.4+0746	02 59 25.9	+07 47 00	0.89	2.41	M	M	M	M
4FGL J0312.8+0134	03 12 53.3	+01 34 21	0.664	2.33	M	N	N	N
4FGL J0339.5-0146	03 39 30.5	-01 46 37	0.85	2.72	M	M	M	M
4FGL J0423.3-0120	04 23 18.2	-01 20 03	0.91609	2.73	M	M	M	M
4FGL J0442.6-0017	04 42 38.7	-00 17 46	0.845	2.78	M	N	M	N
4FGL J0449.2+6329	04 49 16.4	+63 29 40	0.781	2.60	M	N	M	N
4FGL J0505.3+0459	05 05 22.3	+04 59 58	0.59	2.85	M	M	M	M
4FGL J0509.4+1012	05 09 24.2	+10 12 03	0.621	2.41	M	N	M	N
4FGL J0526.2-4830	05 26 17.1	-48 30 54	1.3041	2.55	M	M	M	M
4FGL J0532.6+0732	05 32 41.3	+07 32 57	1.254	2.78	M	M	M	M
4FGL J0532.9-8325	05 32 58.9	-83 25 57	0.774	2.07	M	N	M	N
4FGL J0654.4+4514	06 54 25.4	+45 14 41	0.928	2.57	M	N	M	N
4FGL J0709.7-0255	07 09 46.8	-02 55 48	1.472	2.54	M	N	M	N
4FGL J0719.3+3307	07 19 21.6	+33 07 24	0.779	2.63	M	M	M	M
4FGL J0725.2+1425	07 25 17.8	+14 25 16	1.038	2.58	M	M	M	M
4FGL J0739.2+0137	07 39 16.8	+01 37 18	0.19	2.89	M	M	M	M
4FGL J0742.6+5443	07 42 41.2	+54 43 37	0.723	2.70	M	N	M	N
4FGL J0748.6+2400	07 48 39.3	+24 01 00	0.40932	2.34	M	M	M	M
4FGL J0829.4+0857	08 29 24.8	+08 57 22	0.866	2.06	M	N	M	N
4FGL J0850.1-1212	08 50 09.9	-12 12 44	0.87	2.69	M	M	M	M
4FGL J0909.7-0230	09 09 47.1	-02 30 51	0.957000	2.73	M	N	N	N
4FGL J0921.6+6216	09 21 40.4	+62 16 15	1.447000	2.69	M	N	M	N
4FGL J0922.4-0528	09 22 27.0	-05 28 29	0.974	2.14	M	M	M	N
4FGL J1006.7-2159	10 06 46.3	-21 59 28	0.33	2.57	M	M	M	M
4FGL J1016.0+0512	10 16 02.2	+05 12 32	1.701000	2.22	M	N	M	N
4FGL J1033.1+4115	10 33 06.0	+41 15 43	1.118000	2.41	M	N	M	N
4FGL J1033.9+6050	10 33 56.4	+60 50 57	1.408000	2.56	M	M	M	M
4FGL J1037.4-2933	10 37 25.5	-29 33 24	0.31	2.41	M	N	N	N
4FGL J1043.2+2408	10 43 13.3	+24 08 46	0.560000	2.32	M	M	M	M

Table 2 – *continued*

Sourcename (4FGL-DR2)	R.A.	Decl.	Redshift	Spectral Slope (10 GeV)	CTAO (Omega)		CTAO (Alpha)	
					MFM	FM	MFM	FM
4FGL J1106.0+2813	11 06 00.5	+28 13 31	0.84434	2.37	M	N	M	N
4FGL J1123.4-2529	11 23 28.4	-25 29 17	0.146	2.24	M	M	M	N
4FGL J1127.8+3618	11 27 51.3	+36 18 50	0.8841	2.37	M	N	M	N
4FGL J1146.9+3958	11 46 57.7	+39 58 39	1.087885	2.71	M	M	M	M
4FGL J1153.4+4931	11 53 24.1	+49 31 01	0.33364	2.41	M	M	M	M
4FGL J1154.0+4037	11 54 03.5	+40 37 55	0.92834	2.11	M	N	M	N
4FGL J1246.7-2548	12 46 45.3	-25 48 06	0.63	2.85	M	M	M	M
4FGL J1310.5+3221	13 10 31.8	+32 21 17	0.99725	2.59	M	M	M	M
4FGL J1316.1-3338	13 16 06.0	-33 38 11	1.21	2.62	M	N	M	N
4FGL J1322.2+0842	13 22 12.2	+08 42 13	0.326	2.26	M	N	N	N
4FGL J1345.5+4453	13 45 34.6	+44 53 04	2.542000	2.65	M	M	M	M
4FGL J1349.5-1131	13 49 32.9	-11 31 08	0.340000	2.49	M	N	M	N
4FGL J1401.2-0915	14 01 13.5	-09 15 28	0.667	2.08	M	N	M	N
4FGL J1419.4-0838	14 19 26.4	-08 38 30	0.903	2.56	M	M	M	M
4FGL J1459.5+1527	14 59 33.0	+15 27 51	0.370	2.10	M	N	M	N
4FGL J1512.2+0202	15 12 16.8	+02 02 25	0.21945	2.68	M	M	M	M
4FGL J1522.1+3144	15 22 10.9	+31 44 22	1.4886	2.79	M	M	M	M
4FGL J1549.5+0236	15 49 32.4	+02 36 30	0.41421	2.41	M	M	M	M
4FGL J1625.7-2527	16 25 46.9	-25 27 54	0.79	2.90	M	M	M	M
4FGL J1635.2+3808	16 35 16.0	+38 08 24	1.814000	3.07	M	N	M	N
4FGL J1637.7+4717	16 37 44.2	+47 17 29	0.735000	2.43	M	N	M	N
4FGL J1640.4+3945	16 40 28.6	+39 45 45	1.672000	2.42	M	N	M	N
4FGL J1728.0+1216	17 28 04.8	+12 16 32	0.586	2.45	M	N	N	N
4FGL J1733.0-1305	17 33 03.2	-13 05 09	0.90	2.86	M	M	M	M
4FGL J1734.3+3858	17 34 23.6	+38 58 35	0.975	2.67	M	N	M	N
4FGL J1740.0+4737	17 40 05.4	+47 37 11	0.95	2.10	M	N	M	N
4FGL J1740.5+5211	17 40 32.6	+52 11 34	1.383	2.47	M	N	M	N
4FGL J1802.6-3940	18 02 41.1	-39 40 07	1.319	2.90	M	N	M	N
4FGL J1830.1+0617	18 30 08.7	+06 17 16	0.745	2.37	M	N	M	N
4FGL J1833.6-2103	18 33 38.4	-21 03 27	2.507	2.99	M	N	M	N
4FGL J1849.2+6705	18 49 16.6	+67 05 27	0.66	2.71	M	M	M	M
4FGL J1852.4+4856	18 52 27.8	+48 56 06	1.250	2.29	M	M	M	M
4FGL J2023.6-1139	20 23 36.8	-11 39 31	0.698	2.51	M	M	M	M
4FGL J2025.2+0317	20 25 14.0	+03 17 21	2.210	2.18	M	N	M	N
4FGL J2121.0+1901	21 21 02.4	+19 01 57	2.180	2.43	M	N	M	N
4FGL J2143.5+1743	21 43 34.6	+17 43 50	0.21	2.69	M	M	M	M
4FGL J2147.3-7536	21 47 18.4	-75 36 09	1.14	2.77	M	N	M	N
4FGL J2156.3-0036	21 56 19.1	-00 36 14	0.495	2.25	M	M	M	M
4FGL J2203.4+1725	22 03 29.3	+17 25 54	1.076	2.65	M	N	M	N
4FGL J2225.7-0457	22 25 43.7	-04 57 13	1.404	2.42	M	N	N	N
4FGL J2321.9+2734	23 21 58.1	+27 34 18	1.25	2.15	M	N	M	N
4FGL J2321.9+3204	23 21 54.7	+32 04 25	1.489	2.76	M	N	M	N
4FGL J2323.5-0317	23 23 33.2	-03 17 24	1.41	2.69	M	M	M	N
4FGL J2348.0-1630	23 48 03.8	-16 30 58	0.58	2.57	M	M	M	M

REFERENCES

- Abdo A. A., et al., 2010, *ApJ*, 722, 520
- Abdollahi S., et al., 2020, *ApJS*, 247, 33
- Abeyssekara A. U., et al., 2015, *ApJ*, 815, L22
- Ackermann M., et al., 2012, *Science*, 338, 1190
- Aharonian F., et al., 2006, *A&A*, 457, 899
- Ahnen M. L., et al., 2015, *ApJ*, 815, L23
- Ahnen M. L., et al., 2016, *A&A*, 595, A98
- Aleksić J., et al., 2012, *Astroparticle Physics*, 35, 435
- Aleksić J., et al., 2016, *Astroparticle Physics*, 72, 76
- Antonelli L. A., 2021, *PoS*, ICRC2021, 897
- Atwood W. B., et al., 2009, *ApJ*, 697, 1071
- Ballet J., Burnett T. H., Digel S. W., Lott B., 2020, arXiv e-prints, p. [arXiv:2005.11208](https://arxiv.org/abs/2005.11208)
- Balmaverde B., et al., 2019, *Monthly Notices of the Royal Astronomical Society*, 492, 3728
- Barres de Almeida U., Giacinti G., Longo F., 2021, *PoS*, ICRC2021, 893
- Błażejowski M., Sikora M., Moderski R., Madejski G. M., 2000, *The Astrophysical Journal*, 545, 107
- Blumenthal G. R., Gould R. J., 1970, *Reviews of Modern Physics*, 42, 237
- Burrows D. N., et al., 2005, *Space Sci. Rev.*, 120, 165
- Cao Z., 2021, *PoS*, ICRC2021, 011
- Cherenkov Telescope Array Consortium et al., 2019, Science with the Cherenkov Telescope Array, doi:10.1142/10986.
- Ciprini S., Cheung C. C., 2020, *The Astronomer's Telegram*, 13382, 1
- Costamante L., 2019, *Monthly Notices of the Royal Astronomical Society*, 491, 2771
- Dermer C. D., Schlickeiser R., 1993, *ApJ*, 416, 458
- Domínguez A., et al., 2011, *MNRAS*, 410, 2556
- Dwek E., Krennrich F., 2013, *Astroparticle Physics*, 43, 112
- Foffano L., Prandini E., Franceschini A., Paiano S., 2019, *Monthly Notices of the Royal Astronomical Society*, 486, 1741
- Franceschini A., Rodighiero G., 2017, *Astronomy & Astrophysics*, 603, A34
- Galanti G., Roncadelli M., 2018, *Journal of High Energy Astrophysics*, 20, 1
- Gould R. J., Schröder G. P., 1967, *Physical Review*, 155, 1404
- Gueta O., 2021, arXiv e-prints, p. [arXiv:2108.04512](https://arxiv.org/abs/2108.04512)
- Harrison F. A., et al., 2013, *ApJ*, 770, 103
- HiGRO Collaboration et al., 2021, arXiv e-prints, p. [arXiv:2107.04297](https://arxiv.org/abs/2107.04297)
- Holder J., et al., 2006, *Astroparticle Physics*, 25, 391
- Holler M., De Naurois M., Zaborov D., Balzer A., Chalmé-Calvet R., 2016, *PoS*, ICRC2015, 980
- Irastorza I. G., Redondo J., 2018, *Progress in Particle and Nuclear Physics*, 102, 89
- Jansen F., et al., 2001, *A&A*, 365, L1
- Kirk J. G., Rieger F. M., Mastichiadis A., 1998, *A&A*, 333, 452
- Knödseder J., 2016, *Comptes Rendus Physique*, 17, 663
- MAGIC Collaboration et al., 2021, *A&A*, 647, A163
- Malik Z., Sahayanathan S., Shah Z., Iqbal N., Manzoor A., Bhatt N., 2022, *MNRAS*, 511, 994
- Massaro E., Perri M., Giommi P., Nesci R., 2004, *A&A*, 413, 489
- Massaro F., Paggi A., Errando M., D'Abrusco R., Masetti N., Tosti G., Funk S., 2013, *The Astrophysical Journal Supplement Series*, 207, 16
- Meyer M., Scargle J. D., Blandford R. D., 2019, *ApJ*, 877, 39
- Mirzoyan R., 2017, *The Astronomer's Telegram*, 11061, 1
- Mukherjee R., VERITAS Collaboration 2017, *The Astronomer's Telegram*, 11075, 1
- Paiano S., Treves A., Franceschini A., Falomo R., 2021, *MNRAS*, 508, 6128
- Rajput B., Stalin C. S., Rakshit S., 2020, *A&A*, 634, A80
- Sikora M., Begelman M. C., Rees M. J., 1994, *ApJ*, 421, 153
- Urry C. M., Padovani P., 1995, *Publications of the Astronomical Society of the Pacific*, 107, 803
- Wagner S., Rani B., H. E. S. S. Collaboration 2021, *The Astronomer's Telegram*, 15020, 1
- Zhu K. R., Kang S. J., Zhou R. X., Zheng Y. G., 2021, *ApJ*, 916, 93
- de Naurois M., Mazin D., 2015, *Comptes Rendus Physique*, 16, 610

This paper has been typeset from a $\text{\TeX}/\text{\LaTeX}$ file prepared by the author.